2019

Catalytic Mechanism of Amyloid-β Peptide Degradation by Insulin Degrading Enzyme: Insights from QM/MM MP2 Calculation

Rui Lai
University of Nebraska - Lincoln

Wei-Jen Tang
The University of Chicago

Hui Li
University of Nebraska - Lincoln, hli4@unl.edu

HHS Public Access

Author manuscript

J Chem Inf Model. Author manuscript; available in PMC 2019 August 01.

Published in final edited form as:

J Chem Inf Model. 2018 September 24; 58(9): 1926–1934. doi:10.1021/acs.jcim.8b00406.

Catalytic Mechanism of Amyloid-β Peptide Degradation by Insulin Degrading Enzyme: Insights from QM/MM MP2 Calculation

Rui Lai[1], **Wei-Jen Tang**[2], **Hui Li**[1]

[1]Department of Chemistry, Nebraska Center for Materials and Nanoscience, and Center for Integrated Biomolecular Communication, University of Nebraska-Lincoln, NE 68588-0304

[2]Ben May Department for Cancer Research, The University of Chicago, IL 60637

Abstract

Insulin degrading enzyme (IDE), a metalloprotease that degrades amyloid-β (Aβ) peptides and insulin, is associated with Alzheimer's disease and diabetes. The mechanism of IDE catalyzed degrading of Aβ peptides, which is of fundamental importance in the design of therapeutic methods for Alzheimer's disease, has not been fully understood. In this work, combined quantum mechanics and molecular mechanics (QM/MM) style Møller-Plesset second order perturbation theory (MP2) geometry optimization calculations are performed to investigate the catalytic mechanism of the Aβ40 Phe19-Phe20 peptide bond cleavage by human IDE. The analyses using QM/MM MP2 optimization suggest that a neutral water molecule is at the active site of the enzyme-substrate (ES) complex. The water molecule is in hydrogen bonding with the nearby anionic Glu111 of IDE, but not directly bound to the catalytic Zn ion. This is confirmed by QM/MM DFTB3 molecular dynamics simulation. Our studies also reveal that the hydrolysis of the Aβ40 Phe19-Phe20 peptide bond by IDE consists of four key steps. The neutral water is first activated by moving toward and binding to the Zn ion. A gem-diol intermediate is then formed by the activated neutral water molecule attacking the C atom of the Phe19-Phe20 peptide bond. The next is the protonation of the N atom of Phe19-Phe20 peptide bond to form an intermediate with an elongated C-N bond. The final step is the breaking of the Phe19-Phe20 C-N bond. The final step is the rate-determining step with a calculated Gibbs free energy of activation of 17.34 kcal/mol, in good agreement with the experimental value 16.7 kcal/mol. This mechanism provides the basis for the design of biochemical methods to modulate the activity of IDE in humans.

Graphical Abstract

hli4@unl.edu.

Supporting Information

See supporting information for details of the computational methods and the QM/MM MP2 optimized coordinates of the QM atoms.

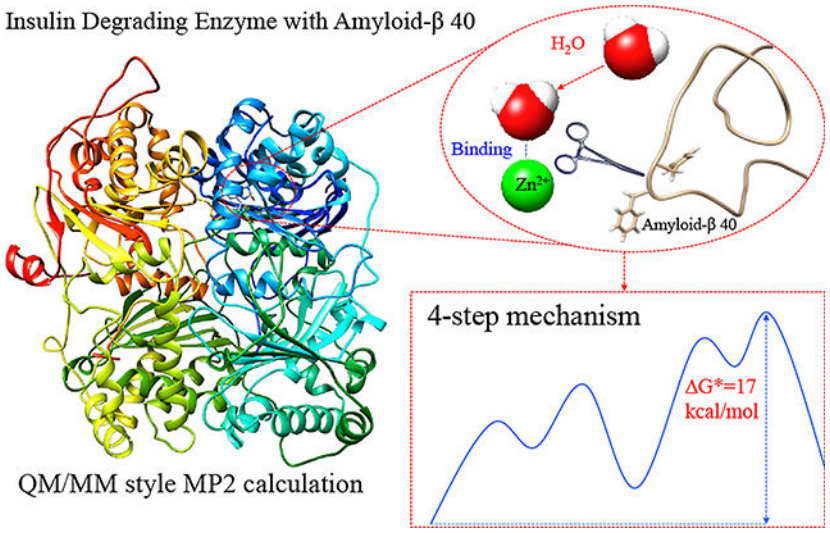

I. Introduction

Insulin degrading enzyme (IDE, EC 3.4.24.56) is an evolutionarily conserved zinc metalloprotease that effectively degrades three pancreatic hormones, insulin, amylin, and glucagon that regulate glucose levels.[1–4] Concordantly, the defects of IDE lead to glucose intolerance in rodents.[5,6] Furthermore, the genome-wide association studies and polymorphism studies reveal that IDE gene is linked to type 2 diabetes in humans.[7,8] IDE also degrades other bioactive, amyloidogenic peptides, such as amyloid β (Aβ).[9] Based on amyloid cascade hypothesis, Aβ aggregates plays a key role in the progression of Alzheimer's disease.[10] The enhancement of IDE activity is a promising therapeutic approach for Alzheimer's disease as IDE degrades the monomeric form of Aβ,[11] which would curtail the Aβ aggregate-mediated toxicity in brain. Consistent with this notion, IDE over-expression reduced Aβ load in mice.[12] A fundamental understanding for the catalytic mechanism of how IDE degrades Aβ would contribute to better design of methods for controlling the degradation of Aβ by IDE.

In general, zinc metalloproteases use zinc ion to activate a water molecule to nucleophilically attack the C atom of a targeted peptide bond. The water molecule can exist as a hydroxide ion (OH^-) in the enzyme-substrate (ES) ground state, or as a neutral water. After the initial nucleophilic attack, the N atom of the targeted peptide bond can accept a proton (H^+). As a result, the peptide C-N bond would be significantly weakened, and finally break. Different metalloproteases and its targeted substrates have been shown to have very different energetics in these catalytic steps.[13] For example, the Zn^{2+}-assisted nucleophilic attack of H_2O or OH^- to C atom could be the rate determining step if the activation free energy is the highest. The proton transfer event could also be rate-determining, and the enzyme catalyzed hydrolysis reaction would show a significant solvent hydrogen-deutorium kinetic isotop effect.[14] In some cases, the peptide C-N bond breaking could also be the rate-determining step. Therefore, it is necessary to identify the specific mechanism of a given pair of zinc protease and substrate in addition to the general acid-base catalytic mechanism. Understanding the specific mechanism can be critical for retional design of small molecule

modulators for a given zinc protease. For example, if the peptide C-N bond breaking is the rate-determining step, an effective small molecule modulator should be able to alter the free energy of activation for the C-N bond breaking.

Kinetic studies show that IDE stochastically cleaves a variety of peptide bonds in Aβ peptides, primarily at Val12-His13, His13-His14, His14-Gln15, Phe19-Phe20, Phe20-Ala21, and Lys28-Gly29.[15] X-ray diffraction method has been used to determine the crystal structure of IDE and its mutants in complex with substrates such as insulin, Aβ peptides and mutated Aβ peptides.[16,17] It is found that the tertiary structure of IDE contains four homologous domains in the form of $\alpha\beta$-sandwich. A flexible loop, formed by 28 residues of IDE, enables open and closed conformations. When it is closed, human IDE forms a catalytic chamber, which consists a Zn^{2+} ion coordinated by three residues, His108, His112 and Glu189.[18] The existence of a distal site, which is ~30 Å away from the active site, serves to anchor Aβ N-terminus, allowing the stochastic cleavages at the middle of Aβ.[18,19] It is worth noting that the Phe19-Phe20 peptide bond is consistently found at the active site in many X-ray crystal structures of IDE in complex with Aβ peptides, for example, in 2G47[16], 4M1C and 2WK3[17].

Theoretical investigations of the catalytic mechanism,[20–22] adenosine triphosphate (ATP) inhibition of IDE,[23] and the interaction between Aβ peptides and IDE[24] have been attempted. The general mechanism of human IDE was studied by Amata *et al*,[20] who used truncated chemical models consisting of 130 and 159 atoms and density functional theory (DFT) method in gas phase and in solvent. The substrates involved in their study were simplified as CH_3NH-Leu-Tyr-Leu-$CONHCH_3$ and CH_3NH-Ala-Ala-Ala-$CONHCH_3$. They found that in the small model corresponding to the enzyme-substrate (ES) state, a hydroxide ion (OH^-) is bound to the Zn^{2+} and forms a hydrogen bond to the nearby neutral Glu111.[20] Bora *et al*[21] used similar methods (DFT and a continuum solvation model) on truncated chemical models (68–80 atoms) of IDE active site with three dipeptides representing His14-Gln15, Phe19-Phe20, Lys28-Gly29. A different ES state was identified in that a neutral water molecule rather than a hydroxide was binding to the Zn^{2+} ion. Bora *et al*'s results suggest that the rate-determining step for the cleavage of these dipeptides is the activation of the neutral water molecule by Zn^{2+} and anionic Glu111 and the simultaneous addition of the resulted hydroxide ion to the peptide C atoms.[21] da Cruz and Seabra used combined quantum mechanics and molecular mechanics (QM/MM[25]) style self-consistent charge density functional tight-binding (i.e., SCC-DFTB[26]) molecular dynamics (MD) simulation method to study the ATP inhibition of IDE in the hydrolysis of the Phe19-Phe20 peptide bond in Aβ42.[22] In their spherical QM/MM system, the QM region had 120 atoms and the MM region had more than 66000 atoms. Similar to Bora *et al*[21], da Cruz *et al*[22] found that the ES state contains a neutral water molecule directly bound to Zn^{2+}. Instead of the hydroxide addition (as the first step), their results suggest that the rate-determining step (as the second step) is the breaking of the Phe19-Phe20 peptide bond in Aβ42 with an activation free energy of 15±2 kcal/mol when ATP is absent, and of 22±4 kcal/mol when ATP is present.

The three theoretical studies aforementioned suggest that either Zn^{2+}-OH^- or Zn^{2+}-H_2O is present in the ES ground state. However, no water coordinated by Zn ion is found in all

substrate-bound IDE crystal structures that represent IDE ES state (i.e., substrate is coordinated by Zn^{2+}). It is likely that a water molecule could not be coordinated by the active site Zn ion when the Zn ion is bound to a peptide substrate such as amyloid and insulin in the ES state. This is consistent with the notion that the geometry of Zn ion coordination at the IDE catalytic site could not allow stable water coordination upon substrate binding. In addition, no water molecule or hydroxide ion was found to bind to the same Zn ion when BDM series of IDE inhibitors developed by Benoit Déprez and colleagues were used. For example, in the X-ray structure 4DTT.PDB[27], both chains A and B have inhibitors (compound BDM41367) bound to the Zn ions, and no water is bound to the Zn ion. In 4RE9.PDB[28], both chains A and B have the inhibitors (compound BDM71290) bound to Zn ion, and no water is bound to Zn ion. In 4IFH.PDB[28] chain B, an inhibitor (compound BDM44619) is bound to the Zn ion and no water is bound to the Zn ion; while the chain A has no inhibitor, and a water is directly bound to the Zn ion. Interestingly, a water molecule was found to be coordinated by catalytic Zn ion and Glu111 of IDE in substrate-free IDE structure (IDE-Y831F; PDB code 2JG4[29]), highlighting the potential role of glutamate 111 in water coordination. Thus, the ES states and the mechanisms proposed by theoretical studies aforementioned would need to be modified and updated.

IDE needs to undergo a large open-closed conformational change to capture and unfold its substrates and release its reaction products. However, most reported IDE structures are trapped in the fully closed state, likely due to the constraints of crystal lattice. Recently, a Fab bound substrate-free IDE reveals a motion at the catalytic domain that would allow IDE to recognize amyloidogenic peptides.[30] As such crystallization condition would likely provide the requisite conformational freedom for IDE catalysis, we thus use a structure of Fab-bound IDE in complex with Aβ40 (PDB code 4M1C) to perform our MD simulation. In this structure, the Phe19-Phe20 peptide carbonyl O atom is bound to the active site Zn ion, and no water molecule is identified near the Zn ion. We performed highly accurate QM/MM Møller–Plesset second order perturbation theory (MP2)[31] geometry optimization calculations to explore the catalytic reaction pathway energetics for the hydrolysis of the Aβ40 Phe19-Phe20 peptide bond. MP2 methods are consistently more accurate than DFT methods for many closed-shell molecules, especially for Zn compounds, and are often used to calibrate DFT methods. In addition, QM/MM density functional tight-binding third-order method (DFTB3)[32] was used to run MD simulations to examine the position and stability of the neutral water molecule in the enzyme-substrate (ES) state. The third-order DFTB3 method with recent parameterization is systematically more accurate than the second-order SCC-DFTB method.[32] The QM/MM calculations were performed with the methods implemented in the quantum chemistry polarizable force field (QuanPol)[33] program, which offers a seamless and full-spectrum combination of various QM and MM methods in a rigorous fashion. As such, the QM/MM MP2 and DFTB3 methods and results are systematically comparable. In this paper, we applied these improved methodologies, which offer more accurate description of the catalytic mechanism of IDE.

II. Computational methods

All force field and quantum chemical calculations were performed with the quantum chemistry polarizable force field (QuanPol)[33] program implemented in the General Atomic and Molecular Electronic Structure System (GAMESS) package.[34,35] The QM/MM MP2 calculations were performed with the parallel MP2 program implemented by Ishimura, Pulay and Nagase *et al*,[36,37] and the QuanPol routines that add MM interactions to the MP2 method.[38] The QM/MM DFTB3[32] method was implemented by the authors in the QuanPol and GAMESS program based on the DFTB3 code implemented by Nishimoto,[39] and the technical details will be published in a separate paper. The details of the computational methods are available in the Supporting Information.

The coordinates of IDE and Aβ40 were obtained from the chain A and chain G of the X-ray structure file 4M1C in the Protein Data Bank.[40] The missing loops in chains A and G were constructed by using the Modeller tool[41] in the Chimera program;[42] The mutated residues in 4M1C were restored by using the Rotamer tool[43] in the Chimera program;[42] H atoms were added by using the Chimera program.[42] A water molecule was manually added to a position near the Zn ion and Glu111. The QuanPol[33] program was used to assign the AMBER[44–46] ff12SB[47] force field to IDE, Aβ40 peptide and the Zn ion. The QuanPol three-point non-polarizable water model QP301[33] was used for the added water molecule at the active site. The IDE-Aβ40 complex was solvated in a 96 Å × 112 Å × 108 Å periodic boundary condition rectangular box, and randomly filled with 60 Na^+ ions, 36 Cl^- ions, and 30320 water molecules. The whole system had 107407 atoms and a zero net charge (Figure 1).

The system was equilibrated by running force field molecular dynamics (MD) simulation for 1.25 ns with a time step size of 1 fs. The last geometry from the force field MD simulation was used for QM/MM geometry optimizations. The 46 atoms of Aβ40 peptide (including atoms of Val18, Phe19, Phe20 and Ala21) and 48 atoms of IDE (including atoms of His108, His112, Glu111 and Glu189, the zinc ions and the water molecule) were defined as QM atoms (Figure 2). As selected, the QM region had a total of 94 atoms and a zero charge (Figure 2). The 94 QM atoms were optimized together with 1709 MM atoms that were within 16 Å to the Zn^{2+} ion (so the total number of atoms optimized was 1803). The same 1803 QM and MM atoms were optimized in different cases so their energies were comparable. The QM/MM geometry optimization was performed with the MP2[31] method, in which the 6–31G* basis set[48] was used for 80 QM atoms and the aug-cc-pVDZ basis set[49,50] was used for 14 most important QM atoms (Figure 2). The QM/MM optimized coordinates of the 94 QM atoms are available in Supporting Information. QM/MM MP2 Hessian calculations (after QM/MM MP2 geometry optimization) were performed by using a partial Hessian method.[51]

The results of the QM/MM MP2 geometry optimization depend on the initial structure from the MM MD simulation. When affordable, it is common to take a set of snapshots from MM MD simulation to perform QM/MM calculations to enhance the sampling. In this study, the active site of IDE is pretty rigid due to the Zn-ligand coordinate bonds. Therefore, unless the protein environment around the active site is dramatically different, the resulted mechanism and energetics should be similar to each other. Here 1803 atoms around the active site

(radius ~16 Å) were fully optimized, so the influence of the initial structure is further reduced. The QM/MM MP2 method is very expensive (10~20 times more costly than DFT methods in terms of computer resource and timing), so it is not very practical at the current stage to perform a set of QM/MM MP2 calculations for the system.

In order to get a better understanding of how the water molecule moves at the active site in the ES state, QM/MM DFTB3 MD simulation was performed. In the DFTB3 method, the parameter set named the Third-Order Parameterization for Organic and Biological systems (3OB-3–1[52–55]) was used. The ES structure for the QM/MM DFTB3 MD simulation was the QM/MM MP2 optimized geometry. This ES structure was equilibrated at 298.15 K and 1.0 bar for 100.0 ps with a time step size 1.0 fs. At the end of this simulation, the Zn-O_{water} distance was 3.92 Å. This very last geometry was then used to run a subsequent QM/MM DFTB3 thermodynamic integration free energy simulation with a series of restricted distances from 3.9 to 2.1 Å between Zn^{2+} ion and O_{water}.

III. Results and discussion

III.A. Water is not directly bound to Zn in the ES ground state

Both QM/MM MP2 and DFTB3 calculations suggest that there is a neutral water molecule at the active site but the water molecule is not directly bound to the Zn^{2+} ion in the enzyme-substrate (ES) ground state. The O atom of the water molecule stays 4.116 Å away from the Zn^{2+} ion in the QM/MM MP2 optimized structure; an average Zn-O_{water} distance of 4.06 Å was observed in a 100 ps QM/MM DFTB3 MD simulation. This result is consistent with X-ray crystal structures in that the Zn ion is bound to an inhibitor.

Three possible ES candidate structures, A, B and C (Figures 2A, 2B, 2C), were examined with QM/MM MP2 geometry optimization methods. The key interatomic distances and relative energies of these three structures are shown in Table 1. It turned out that structure A is the ES state (and very similar to the X-ray structure 4M1C), structure C is a higher energy (higher than structure A by 7.41 kcal/mol) pre-attack state (named ES* here and hereafter). In order for the neutral water molecule in structure A (the ES state) to attack the C_{Phe19} atom, it should move closer to the C_{Phe19} atom and bind to the Zn^{2+} ion to form structure C (the ES* state), in which it would remain as a neutral water molecule.

Structure A was optimized starting from the last geometry of the force field MD simulation as described in the Computational Methods section. After QM/MM MP2 optimization, the water molecule remains at a position far away from Zn^{2+}, with a distance of 4.12 Å between O and Zn^{2+} (Figure 2A). This water molecule is also far away from the C atom of Phe19, with a distance of 4.250 Å between C_{Phe19} and O_{water}. At this distance, the water molecule is not ready to attack the C_{Phe19} atom and it is difficult to be activated either by the nearby Glu111 or the Zn^{2+} ion. The direct addition of the water molecule to the C_{Phe19} atom of Aβ40 would require a very high activation energy. The structure A has interatomic distances (Zn-$O_{1,\ Glu189}$ 1.95 Å, Zn-$O_{2,\ Glu189}$ 2.47 Å and Zn-O_{Phe19} 2.03 Å) similar to those (Zn-$O_{1,\ Glu189}$: 2.26 Å, Zn-$O_{2,\ Glu189}$: 2.68 Å and Zn-O_{Phe19}: 2.20 Å) in the X-ray structure 4M1C, suggesting that the X-ray structure 4M1C (with Gln111 and other site mutations) may be very similar to the ES state formed by the wild-type IDE. QM/MM DFTB3 MD

simulation was performed for the ES state (Figure 2A) identified from QM/MM MP2 geometry optimization. During the 100.0 ps simulation, the water molecule was wandering in the pocket formed by Glu111 and Aβ40 peptide, but did not bind to Zn^{2+} ion. The water molecule maintained a hydrogen bond with the anionic Glu111 thus could not flee from the active center. The average distance between the O atom of the water molecule and the Zn^{2+} ion was 4.06 Å, with the shortest (note the distances were checked at every 1000 fs) distance being 2.72 Å and the longest distance being 5.67 Å. For comparison, when a neutral water molecule binds to a Zn ion, the O-Zn distance should be ~2.0 Å. Therefore, both QM/MM geometry optimization and MD simulation suggest that the neutral water molecule is not bound to Zn^{2+} ion and its position is not fixed, making it difficult to be identified in X-ray diffraction measurement of IDE crystal structures.

Structure B was started from a structure in that the water molecule is manually positioned to be close to the C atom of Aβ40 Phe19, thus ready to react. As positioned, the water molecule is not bound to the Zn^{2+} ion (with a Zn-O_{water} distance ~4 Å). After optimization the water molecule remains at the initially assigned position (Figure 2B), with a Zn-O_{water} distance of 4.164 Å and a distance between C_{Phe19} and O_{water} being 2.513 Å. Structure B (Figure 2B) is 8.79 kcal/mol higher in energy than structure A.

Structure C was similar to structure B, but the water molecule was manually positioned to bind to the Zn^{2+} (with a Zn-O_{water} distance ~2 Å). In addition, an H atom of the water molecule was manually moved to Glu111 so the neutral water became a hydroxide ion and Glu111 was neutral. This is to examine whether a hydroxide can directly bind to the Zn ion in the ES state. This structure was then optimized with the QM/MM MP2 method. During the optimization process, the proton on Glu111 automatically transferred back to the hydroxide to form a neutral water molecule and an anionic Glu111 (Figure 2C). The Zn-O_{water} distance was optimized to 2.028 Å. Due to the binding of the neutral water to the Zn ion, the binding between Aβ40 O_{Phe19} and the Zn^{2+} ion is lost (becomes 3.37 Å), so the Zn^{2+} ion retains the same coordination number. This is probably due to steric effects. This result suggests that a hydroxide ion is not preferred at the active center, even when it is bound to Zn^{2+}. In structure C, the distance between the C atom of Phe19 (C_{Phe19}) and the O atom of the neutral water molecule (O_{water}) is 2.62 Å, so the water is ready to attack the C_{Phe19}.

III.B. Four-step mechanism

Our computational results support a four-step catalytic mechanism with the rate-determining step being the breaking of the Aβ40 Phe19-Phe20 peptide bond (C-N bond) concerted with a proton transfer to Glu111 of IDE. The details of the proposed catalytic mechanism are shown in Figure 3 and the electronic energy profile is shown in Figure 4.

The first step is the evolving of ES (Figure 2A and Figure 3) to ES* (Figure 2C and Figure 3), which involves the breaking and formation of Zn^{2+} coordinate bonds. As already discussed, the ES* state is higher in energy then the ES state by 7.41 kcal/mol as calculated with the QM/MM MP2 optimization method. In order to estimate the Gibbs free energy change (ΔG) from ES to ES*, a thermodynamic integration free energy simulation was performed using the QM/MM DFTB3 method. In the DFTB3 free energy simulation, the

$Zn\text{-}O_{water}$ distances were gradually changed from 3.9 Å (ES state) to 2.1 Å (ES* state). Figure 5 shows that the ES* state (Figure 2C) has a higher Gibbs free energy (4.86 kcal/mol higher) than the ES state (Figure 2A). This is in fairly good agreement with the QM/MM MP2 geometry optimization result 7.41 kcal/mol. The ES* state from this QM/MM DFTB3 simulation is similar to the ES* state found from QM/MM MP2 optimization: all Zn-ligand distances are similar except for the $Zn\text{-}O_{Phe19}$ distance (DFTB3 is ~2.37 Å while MP2 is 3.372 Å). As discussed earlier, the Aβ40 O_{Phe19} ligand steps away as the water establishes a direct binding to the Zn^{2+} ion. The QM/MM DFTB3 simulation shows a similar trend: the $Zn\text{-}O_{Phe19}$ distance increases from 1.99 Å (in ES state, water not binding to Zn) to 2.37 Å (ES*, with water binding to Zn). A search for the transition state linking ES and ES* was attempt with the QM/MM MP2 method, but it turned out that these two states are far away on the potential energy surface so it is very difficult to find a well-defined transition state between them. There must be several transition states between them. The QM/MM DFTB3 MD free energy simulation suggests that the free energy of activation for ES conversion to ES* is 5.52 kcal/mol (Figure 5). Nevertheless, the conformational changes on going from ES to ES* to kick off the degradation of Aβ40 peptide is very unlikely the rate-determining step.

In the second step, as the neutral water molecule is already bound to the Zn^{2+} ion (the ES* state), it is ready to attack the Phe19-Phe20 peptide bond. The first transition state (T1) is formed with a reduction of the distance (2.62 Å to 1.91 Å) between the C atom of Phe19 (C_{Phe19}) and the O atom of the neutral water molecule (O_{water}). In the meantime, an H atom of the water transfers to Glu111. The electronic energy barrier calculated for this process is 13.69 kcal/mol (Figure 4). Passing this transition state, an intermediate EI1 is formed with a $C_{Phe19}\text{-}O_{water}$ bond length of 1.49 Å and a neutral Glu111. The electronic energy for EI1 is higher than the ES state by +4.29 kcal/mol.

In the third step, Glu111 delivers the just accepted H atom to the N of Phe20 (N_{Phe20}). The distance between H and N_{Phe20} is reduced from 2.94 Å (in EI1) to 1.09 Å (in EI2) with a transition state distance of 1.28 Å (in T2). The electronic energy barrier for this step is calculated as 16.73 kcal/mol. Due to the formation of the N-H bond, the substrate $C_{Phe19}\text{-}N_{Phe20}$ peptide bond is significantly weakened as the bond length changes from 1.46 Å in EI1 to 1.55 Å in T2, and to 1.60 Å in EI2.

In the fourth step, the weakened $C_{Phe19}\text{-}N_{Phe20}$ peptide bond breaks by passing a transition state T3 to reach the final product PS. Concertedly, the other H atom of the H_2O molecule (now carboxylic acid proton on Phe19) transfers to the anionic Glu111, making it neutral. The electronic energy barrier calculated for this step is 17.68 kcal/mol, higher than other steps. So this is the rate-determining step. Partial Hessian analysis was performed and the free energy correction was calculated as −0.34 kcal/mol, with a −1.27 kcal/mol contribution from zero point energy. Therefore, the activation free energy can be estimated as 17.34 kcal/mol.

III.C. Comparison to experimental kinetics

Leissring *et al*[15] determined the rate of degradation of Aβ peptide by IDE by using modified Aβ peptide (fluorescein-Aβ-(1–40)-Lys-biotin) and two different methods: fluorescence

polarization (FP) and avidin-agarose precipitation (AAP), which yielded k_{cat} as 256±22 min $^{-1}$ and 221±11 min^{-1}, respectively. According to unimolecular transition state theory, those rate constants correspond to activation free energies of 16.59±0.05 kcal/mol and 16.68±0.03 kcal/mol for FP and AAP, respectively. Our calculated activation free energy is 17.34 kcal/mol, which is in good agreement with these experimental values. While the agreement is good, we must note that the experimentally measured rate constant is for modified Aβ peptide assay instead of the wild-type Aβ peptide. Moreover, the measured rate constant is not solely for the degradation of Aβ peptide at Phe19-Phe20 position because Aβ peptide can be degraded by IDE at several possible positions, such as Lys28-Gly29 and His14-Gln15.

III.D. Comparison to other theoretical results

Amata *et al*.[20] reported that the cleavage of peptide bonds involves an OH^- nucleophilic addition with activation free energies of 15.9 kcal/mol for Ala-Ala and 15.6 kcal/mol for Tyr-Leu. The highest transition state found in their study is the TS2 (corresponding to OH^- addition to the peptide N atom), so the rate-determining free energy of activation are 19.2 and 19.5 kcal/mol, respectively. Bora *et al*.[21] suggested that the rate-determining step is the activation of the neutral water molecule by Zn^{2+} and anionic Glu111 and the simultaneous addition of the resulted hydroxide ion to the peptide C atoms.[21] The electronic energy barrier of this step calculated for the His14-Gln15, Phe19-Phe20, Lys28-Gly29 dipeptide models are 22.3, 18.8 and 14.3 kcal/mol, respectively.[21] Both of these papers suggest that the rate-determining step is the OH^- addition to the peptide C atom. The QM/MM MP2 calculation in the current paper suggests that the OH^- addition step requires an electronic energy barrier of 13.69 kcal/mol, and is not the rate-determining step. While these comparisons are meaningful, because there could be a common catalytic mechanism for different substrates, we must emphasize that the mechanism and energetics may be very different for small peptides and long peptides. In addition, different QM methods (DFT v.s. MP2) may also give different results.

da Cruz and Seabra used QM/MM SCC-DFTB molecular dynamics (MD) simulation method to study the IDE hydrolysis of the Phe19-Phe20 peptide bond in Aβ42.[22] Instead of the hydroxide addition, their results suggest that the rate-determining step is the breaking of the Phe19-Phe20 peptide N-C bond in Aβ42, with an activation free energy of 15±2 kcal/mol when ATP is absent, and of 22±4 kcal/mol when ATP is present. The QM/MM MP2 calculation in the current paper also suggests that the rate-determining step is the N-C bond breaking, with a 17.34 kcal/mol free energy of activation (but note the two different substrates: Aβ42 versus Aβ40).

These comparisons suggest that the choice of QM/continuum and QM/MM methods may significantly affect the computed reaction energetics: QM/continuum methods may overestimate the OH^- addition energy barrier.

IV. Conclusion

QM/MM MP2 and DFTB3 methods are used to investigate the catalytic mechanism of hydrolysis of the Phe19-Phe20 peptide bond in Aβ40 by insulin degrading enzyme (IDE). It

is found that in the enzyme-substrate (ES) state, the reactive water molecule is not directly bound to Zn^{2+} ion, different from the findings in other theoretical studies.[20–22] The distance between the O atom of the water molecule is 4.116 Å in the MP2/[aug-cc-pVDZ/6–31G*]/AMBER optimized structure. QM/MM DFTB3 MD simulation suggests that this water molecule can move around at the active center. The average distance between O atom of H_2O molecule and the Zn^{2+} ion is calculated to be 4.06 Å during the 100 ps simulation with the shortest distance being 2.72 Å and the longest distance being 5.67 Å.

The catalytic reaction can be divided into four steps. In the first step, with the assistance of the anionic Glu111, the neutral water molecule (in hydrogen bond with anionic Glu111) near the active center is activated by binding to the Zn^{2+} ion. In the second step, the activated neutral water molecule attacks the C atom of Aβ40 Phe19-Phe20 peptide bond to form a gem-diol intermediate. In the third step, a proton transfer from Glu111 of IDE to N atom of Aβ40 Phe19-Phe20 peptide bond to form an intermediate with elongated C-N bond that is ready to break. In the fourth step, the peptide C-N bond breaks with a simultaneous proton transfer to Glu111. The fourth step is the rate-determining step with a Gibbs free energy of activation of 17.34 kcal/mol, in good agreement with experimental value 16.6 kcal/mol.

Supplementary Material

Refer to Web version on PubMed Central for supplementary material.

Acknowledgment

This project is supported by a seed grant from the Nebraska Center for Integrated Biomolecular Communication (NIH National Institutes of General Medical Sciences P20-GM113126) and a grant-in-aids from the University of Nebraska-Lincoln Research Council (WBS # 26-0509-9001-016) to H. Li, and the NIH grants GM81539 and GM121964 to W.-J. Tang. The calculations were performed with resources at the University of Nebraska-Lincoln Holland Computing Center.

References

(1). Tundo GR; Sbardella D; Ciaccio C; Grasso G; Gioia M; Coletta A; Polticelli F; Di Pierro D; Milardi D; Van Endert P; Marini S; Coletta M: Multiple functions of insulin-degrading enzyme: a metabolic crosslight? Crit Rev Biochem Mol Biol 2017, 52, 554–582. [PubMed: 28635330]

(2). Tang WJ: Targeting Insulin-Degrading Enzyme to Treat Type 2 Diabetes Mellitus. Trends Endocrin Met 2016, 27, 24–34.

(3). Malito E; Hulse RE; Tang WJ: Amyloid β-degrading cryptidases: insulin degrading enzyme, presequence peptidase, and neprilysin. Cell Mol. Life Sci. 2008, 65, 2574–85. [PubMed: 18470479]

(4). Duckworth WC; Bennett RG; Hamel FG: Insulin degradation: progress and potential. Endocr. Rev. 1998, 19, 608–24. [PubMed: 9793760]

(5). Farris W; Mansourian S; Chang Y; Lindsley L; Eckman EA; Frosch MP; Eckman CB; Tanzi RE; Selkoe DJ; Guenette S: Insulin-degrading enzyme regulates the levels of insulin, amyloid beta-protein, and the beta-amyloid precursor protein intracellular domain in vivo. Proc. Natl. Acad. Sci. U.S.A. 2003, 100, 4162–7. [PubMed: 12634421]

(6). Farris W; Mansourian S; Leissring MA; Eckman EA; Bertram L; Eckman CB; Tanzi RE; Selkoe DJ: Partial loss-of-function mutations in insulin-degrading enzyme that induce diabetes also impair degradation of amyloid beta-protein. Am. J. Pathol. 2004, 164, 1425–34. [PubMed: 15039230]

(7). Karamohamed S; Demissie S; Volcjak J; Liu CY; Heard-Costa N; Liu J; Shoemaker CM; Panhuysen CI; Meigs JB; Wilson P; Atwood LD; Cupples LA; Herbert A: Polymorphisms in the insulin-degrading enzyme gene are associated with type 2 diabetes in men from the NHLBI Framingham Heart Study. Diabetes 2003, 52, 1562–1567. [PubMed: 12765971]

(8). Sladek R; Rocheleau G; Rung J; Dina C; Shen L; Serre D; Boutin P; Vincent D; Belisle A; Hadjadj S; Balkau B; Heude B; Charpentier G; Hudson TJ; Montpetit A; Pshezhetsky AV; Prentki M; Posner BI; Balding DJ; Meyre D; Polychronakos C; Froguel P: A genome-wide association study identifies novel risk loci for type 2 diabetes. Nature 2007, 445, 881–5. [PubMed: 17293876]

(9). Kurochkin IV: Insulin-degrading enzyme: embarking on amyloid destruction. Trends in biochemical sciences 2001, 26, 421–425. [PubMed: 11440853]

(10). Hardy JA; Higgins GA: Alzheimer's disease: the amyloid cascade hypothesis. Science 1992, 256, 184–5. [PubMed: 1566067]

(11). Tseng BP; Esler WP; Clish CB; Stimson ER; Ghilardi JR; Vinters HV; Mantyh PW; Lee JP; Maggio JE: Deposition of monomeric, not oligomeric, Aβ mediates growth of Alzheimer's disease amyloid plaques in human brain preparations. Biochemistry 1999, 38, 10424–10431. [PubMed: 10441137]

(12). Leissring MA; Farris W; Chang AY; Walsh DM; Wu X; Sun X; Frosch MP; Selkoe DJ: Enhanced proteolysis of beta-amyloid in APP transgenic mice prevents plaque formation, secondary pathology, and premature death. Neuron 2003, 40, 1087–93. [PubMed: 14687544]

(13). Zhang T; Ozbil M; Barman A; Paul TJ; Bora RP; Prabhakar R: Theoretical Insights into the Functioning of Metallopeptidases and Their Synthetic Analogues. Accounts of Chemical Research 2015, 48, 192–200. [PubMed: 25607542]

(14). Wang Z; Benkovic SJ: Purification, Characterization, and Kinetic Studies of a SolubleBacteroides fragilis Metallo-β-lactamase That Provides Multiple Antibiotic Resistance. Journal of Biological Chemistry 1998, 273, 22402–22408. [PubMed: 9712862]

(15). Leissring MA; Lu A; Condron MM; Teplow DB; Stein RL; Farris W; Selkoe DJ: Kinetics of amyloid β-protein degradation determined by novel fluorescence-and fluorescence polarization-based assays. Journal of Biological Chemistry 2003, 278, 37314–37320. [PubMed: 12867419]

(16). Shen Y; Joachimiak A; Rosner MR; Tang W-J: Structures of human insulin-degrading enzyme reveal a new substrate recognition mechanism. Nature 2006, 443, 870–874. [PubMed: 17051221]

(17). Guo Q; Manolopoulou M; Bian Y; Schilling AB; Tang W-J: Molecular basis for the recognition and cleavages of IGF-II, TGF-α, and amylin by human insulin-degrading enzyme. Journal of molecular biology 2010, 395, 430–443. [PubMed: 19896952]

(18). Manolopoulou M; Guo Q; Malito E; Schilling AB; Tang W-J: Molecular basis of catalytic chamber-assisted unfolding and cleavage of human insulin by human insulin-degrading enzyme. Journal of Biological Chemistry 2009, 284, 14177–14188. [PubMed: 19321446]

(19). Noinaj N; Bhasin SK; Song ES; Scoggin KE; Juliano MA; Juliano L; Hersh LB; Rodgers DW: Identification of the allosteric regulatory site of insulysin. PloS one 2011, 6, e20864. [PubMed: 21731629]

(20). Amata O; Marino T; Russo N; Toscano M: Human insulin-degrading enzyme working mechanism. Journal of the American Chemical Society 2009, 131, 14804–14811. [PubMed: 19785409]

(21). Bora RP; Ozbil M; Prabhakar R: Elucidation of insulin degrading enzyme catalyzed site specific hydrolytic cleavage of amyloid β peptide: a comparative density functional theory study. JBIC Journal of Biological Inorganic Chemistry 2010, 15, 485–495. [PubMed: 20033747]

(22). da Cruz CH; Seabra G d. M.: QM/MM Simulations of Amyloid-β 42 Degradation by IDE in the Presence and Absence of ATP. Journal of chemical information and modeling 2015, 55, 72–83. [PubMed: 25539133]

(23). da Cruz CH; Seabra G: Molecular Dynamics Simulations Reveal a Novel Mechanism for ATP Inhibition of Insulin Degrading Enzyme. Journal of chemical information and modeling 2014, 54, 1380–1390. [PubMed: 24697863]

(24). Bora RP; Prabhakar R: Elucidation of Interactions of Alzheimer Amyloid β Peptides (Aβ40 and Aβ42) with Insulin Degrading Enzyme: A Molecular Dynamics Study. Biochemistry 2010, 49, 3947–3956. [PubMed: 20380468]

(25). Warshel A; Levitt M: Theoretical studies of enzymic reactions: Dielectric, electrostatic and steric stabilization of the carbonium ion in the reaction of lysozyme. Journal of Molecular Biology 1976, 103, 227–249. [PubMed: 985660]

(26). Elstner M; Porezag D; Jungnickel G; Elsner J; Haugk M; Frauenheim T; Suhai S; Seifert G: Self-consistent-charge density-functional tight-binding method for simulations of complex materials properties. Physical Review B 1998, 58, 7260.

(27). Charton J; Gauriot M; Guo Q; Hennuyer N; Marechal X; Dumont J; Hamdane M; Pottiez V; Landry V; Sperandio O: Imidazole-derived 2-[N-carbamoylmethyl-alkylamino] acetic acids, substrate-dependent modulators of insulin-degrading enzyme in amyloid-β hydrolysis. European journal of medicinal chemistry 2014, 79, 184–193. [PubMed: 24735644]

(28). Deprez-Poulain R; Hennuyer N; Bosc D; Liang WG; Enée E; Marechal X; Charton J; Totobenazara J; Berte G; Jahklal J: Catalytic site inhibition of insulin-degrading enzyme by a small molecule induces glucose intolerance in mice. Nature communications 2015, 6.

(29). Im H; Manolopoulou M; Malito E; Shen Y; Zhao J; Neant-Fery M; Sun C-Y; Meredith SC; Sisodia SS; Leissring MA; Tang W-J: Structure of Substrate-free Human Insulin-degrading Enzyme (IDE) and Biophysical Analysis of ATP-induced Conformational Switch of IDE. Journal of Biological Chemistry 2007, 282, 25453–25463. [PubMed: 17613531]

(30). McCord LA; Liang WG; Dowdell E; Kalas V; Hoey RJ; Koide A; Koide S; Tang WJ: Conformational states and recognition of amyloidogenic peptides of human insulin-degrading enzyme. Proc Natl Acad Sci U S A 2013, 110, 13827–32. [PubMed: 23922390]

(31). Møller C; Plesset MS: Note on an Approximation Treatment for Many-Electron Systems. Physical Review 1934, 46, 618–622.

(32). Gaus M; Cui Q; Elstner M: DFTB3: extension of the self-consistent-charge density-functional tight-binding method (SCC-DFTB). J. Chem. Theory Comput 2011, 7, 931–948.

(33). Thellamurege NM; Si D; Cui F; Zhu H; Lai R; Li H: QuanPol: A full spectrum and seamless QM/MM program. Journal of Computational Chemistry 2013, 34, 2816–2833. [PubMed: 24122765]

(34). Schmidt MW; Baldridge KK; Boatz JA; Elbert ST; Gordon MS; Jensen JH; Koseki S; Matsunaga N; Nguyen KA; Su SJ; Windus TL; Dupuis M; Montgomery JA: General Atomic and Molecular Electronic-Structure System. Journal of Computational Chemistry 1993, 14, 1347–1363.

(35). Gordon MS; Schmidt MW: Advances in electronic structure theory: GAMESS a decade later In Theory and applications of computational chemistry; Dykstra CE, Frenking G, Kim KS, Scuseria GE, Eds.; Elsevier: Amsterdam, 2005.

(36). Ishimura K; Pulay P; Nagase S: A new parallel algorithm of MP2 energy calculations. Journal of Computational Chemistry 2006, 27, 407–413. [PubMed: 16419017]

(37). Ishimura K; Pulay P; Nagase S: New parallel algorithm for MP2 energy gradient calculations. Journal of Computational Chemistry 2007, 28, 2034–2042. [PubMed: 17450568]

(38). Li H: Analytic Energy Gradient in Combined Second-Order Moller-Plesset Perturbation Theory and Polarizable Force Field Calculation. Journal of Physical Chemistry A 2011, 115, 11824–11831.

(39). Nishimoto Y: DFTB/PCM Applied to Ground and Excited State Potential Energy Surfaces. The Journal of Physical Chemistry A 2016, 120, 771–784. [PubMed: 26761635]

(40). Berman HM; Westbrook J; Feng Z; Gilliland G; Bhat TN; Weissig H; Shindyalov IN; Bourne PE: The Protein Data Bank. Nucleic Acids Research 2000, 28, 235–242. [PubMed: 10592235]

(41). Webb B; Sali A: Comparative protein structure modeling using Modeller. Current protocols in bioinformatics 2014, 5.6. 1–5.6. 32.

(42). Pettersen EF; Goddard TD; Huang CC; Couch GS; Greenblatt DM; Meng EC; Ferrin TE: UCSF Chimera—A visualization system for exploratory research and analysis. Journal of Computational Chemistry 2004, 25, 1605–1612. [PubMed: 15264254]

(43). Dunbrack RL: Rotamer Libraries in the 21 st Century. Current opinion in structural biology 2002, 12, 431–440. [PubMed: 12163064]

(44). Cieplak P; Caldwell J; Kollman P: Molecular mechanical models for organic and biological systems going beyond the atom centered two body additive approximation: Aqueous solution free energies of methanol and N-methyl acetamide, nucleic acid base, and amide hydrogen bonding and chloroform/water partition coefficients of the nucleic acid bases. Journal of Computational Chemistry 2001, 22, 1048–1057.

(45). Case DA; Cheatham TE; Darden T; Gohlke H; Luo R; Merz KM; Onufriev A; Simmerling C; Wang B; Woods RJ: The Amber biomolecular simulation programs. Journal of Computational Chemistry 2005, 26, 1668–1688. [PubMed: 16200636]

(46). Wang ZX; Zhang W; Wu C; Lei HX; Cieplak P; Duan Y: Strike a balance: Optimization of backbone torsion parameters of AMBER polarizable force field for simulations of proteins and peptides. Journal of Computational Chemistry 2006, 27, 781–790. [PubMed: 16526038]

(47). Maier JA; Martinez C; Kasavajhala K; Wickstrom L; Hauser KE; Simmerling C: ff14SB: improving the accuracy of protein side chain and backbone parameters from ff99SB. Journal of chemical theory and computation 2015, 11, 3696–3713. [PubMed: 26574453]

(48). Francl MM; Pietro WJ; Hehre WJ; Binkley JS; Gordon MS; Defrees DJ; Pople JA: Self-Consistent Molecular-Orbital Methods .23. A Polarization-Type Basis Set for 2nd-Row Elements. Journal of Chemical Physics 1982, 77, 3654–3665.

(49). Dunning TH: Gaussian basis sets for use in correlated molecular calculations. I. The atoms boron through neon and hydrogen. Journal of Chemical Physics 1989, 90, 1007–1023.

(50). Balabanov NB; Peterson KA: Systematically convergent basis sets for transition metals. I. All-electron correlation consistent basis sets for the 3d elements Sc–Zn. The Journal of Chemical Physics 2005, 123, 064107.

(51). Li H; Jensen JH: Partial Hessian vibrational analysis: the localization of the molecular vibrational energy and entropy. Theoretical Chemistry Accounts 2002, 107, 211–219.

(52). Gaus M; Goez A; Elstner M: Parametrization and Benchmark of DFTB3 for Organic Molecules. Journal of Chemical Theory and Computation 2013, 9, 338–354. [PubMed: 26589037]

(53). Kubillus M; Kubař T; Gaus M; Řezáč J; Elstner M: Parameterization of the DFTB3 Method for Br, Ca, Cl, F, I, K, and Na in Organic and Biological Systems. Journal of Chemical Theory and Computation 2015, 11, 332–342. [PubMed: 26889515]

(54). Gaus M; Lu X; Elstner M; Cui Q: Parameterization of DFTB3/3OB for Sulfur and Phosphorus for Chemical and Biological Applications. Journal of Chemical Theory and Computation 2014, 10, 1518–1537. [PubMed: 24803865]

(55). Lu X; Gaus M; Elstner M; Cui Q: Parametrization of DFTB3/3OB for Magnesium and Zinc for Chemical and Biological Applications. The Journal of Physical Chemistry B 2015, 119, 1062–1082. [PubMed: 25178644]

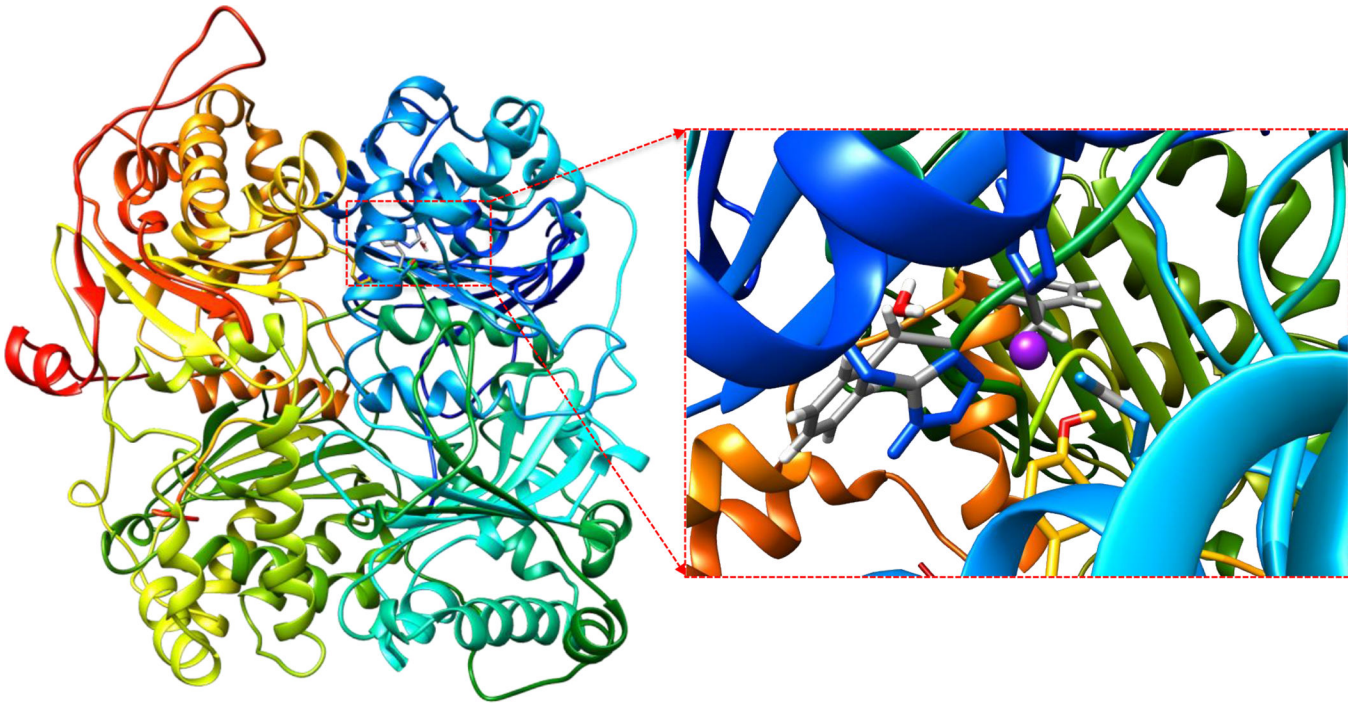

Figure 1.

Structure of QM/MM MP2 optimized enzyme-substrate (ES) state of IDE in complex with Aβ40. The active site structure is shown on the right side. The water molecule is not bound to the Zn^{2+} ion (Zn-O_{water} distance is 4.116 Å). Zn^{2+} ion is displayed in purple. Water molecule is displayed with red (O) and white (H).

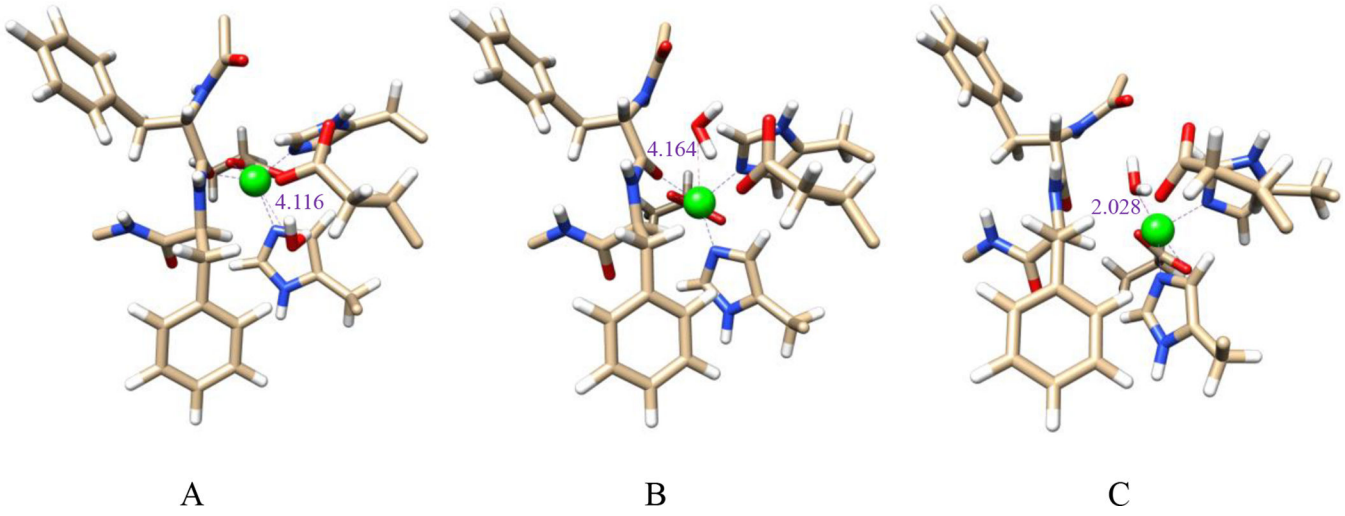

Figure 2.

QM/MM MP2 optimized structure (QM region, 94 atoms in the QM/MM system, Zn: green; N: blue; O: red; C: tan; H: white) for three possible active site structures of the enzyme-substrate (ES) state in the degradation of Aβ40 Phe19-Phe20 peptide bond by IDE. The distance between the O atom of water and the Zn^{2+} ion is: (A) 4.116 Å; (B) 4.164 Å; (C) 2.028 Å.

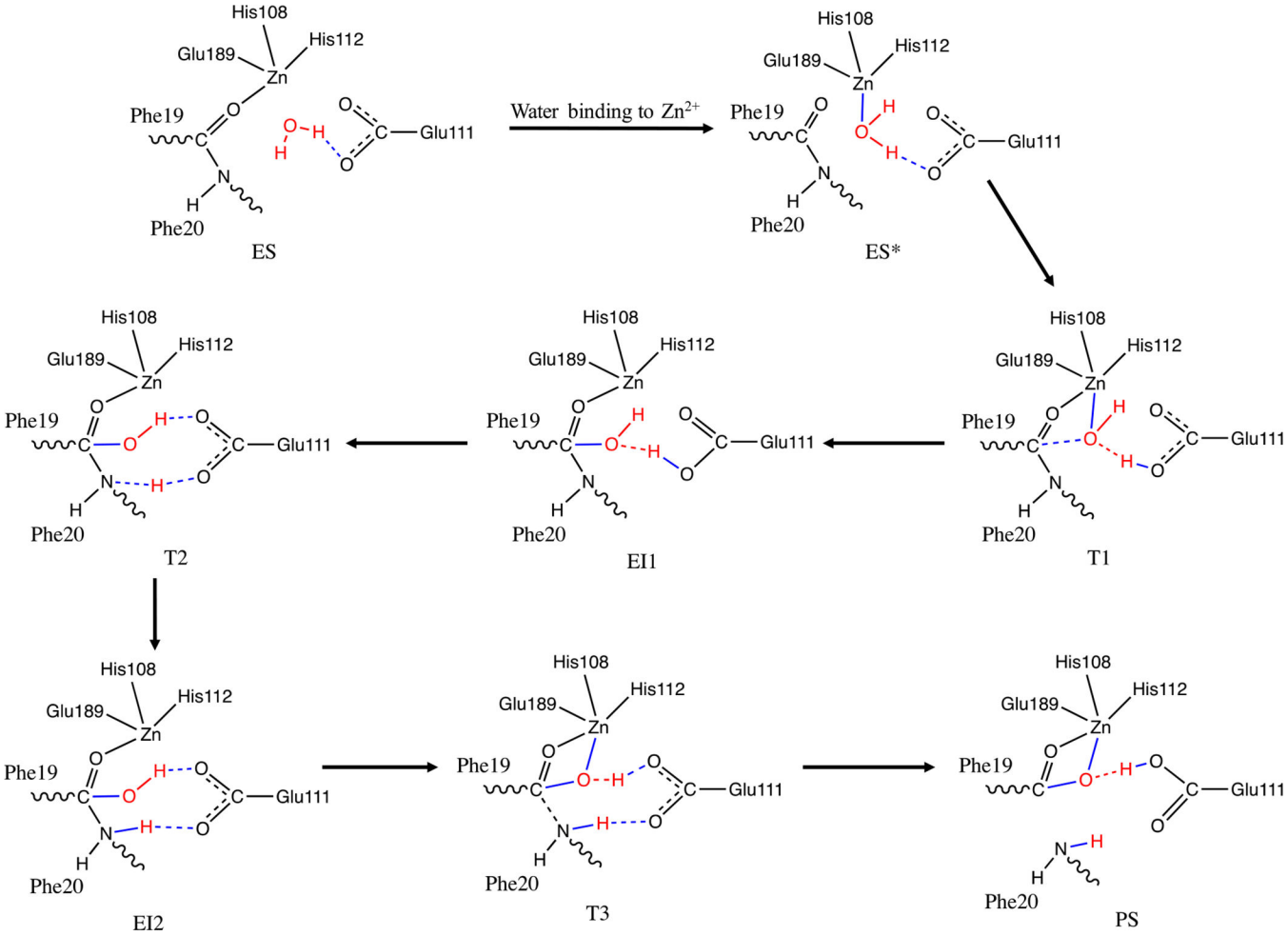

Figure 3.

QM/MM MP2 calculated catalytic mechanism for IDE catalyzed hydrolysis of Aβ40 Phe19-Phe20 peptide bond.

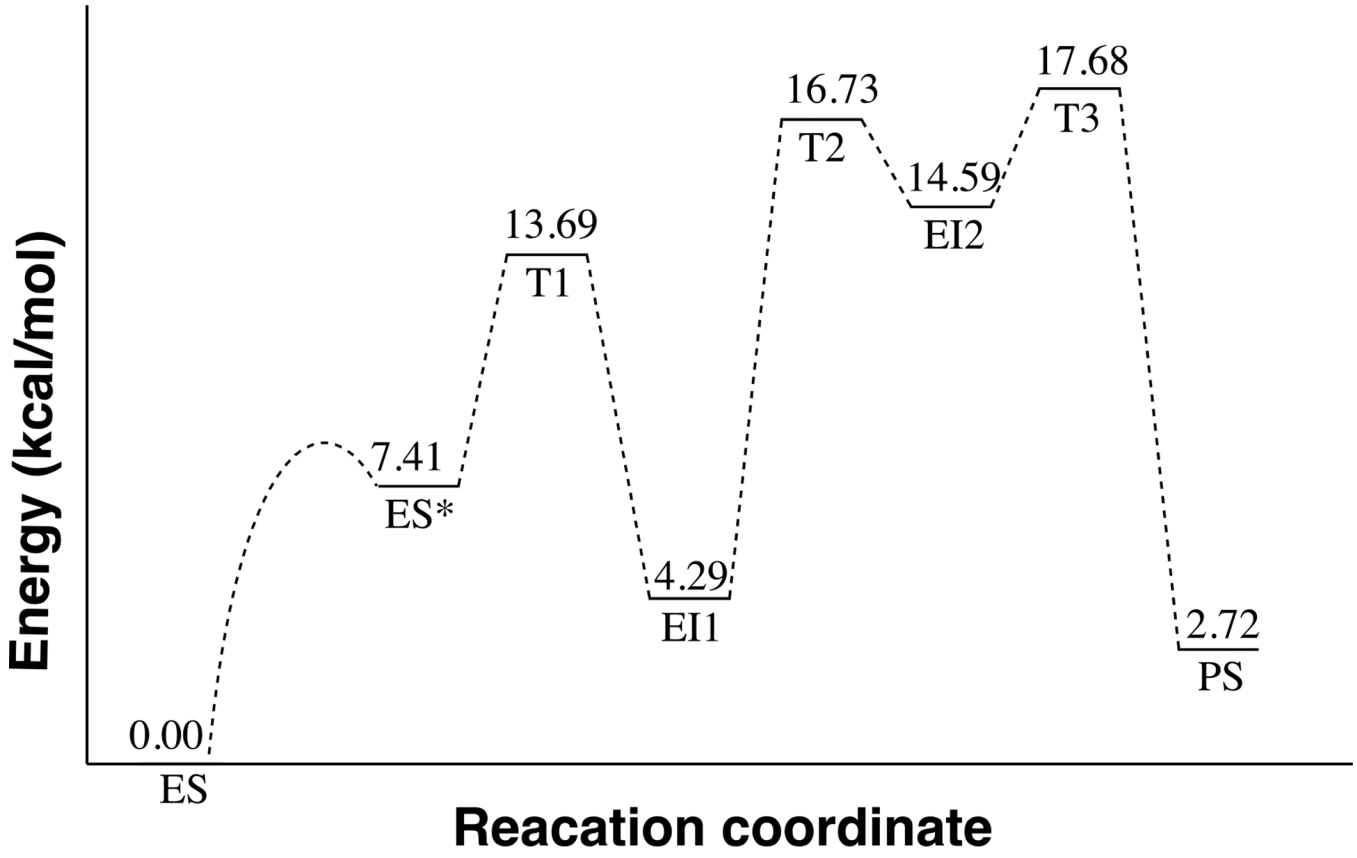

Figure 4.
Electronic energy profiles from QM/MM MP2/[aug-cc-pVDZ/6–31G*] geometry optimization. Zero point energy and thermal energies are not included.

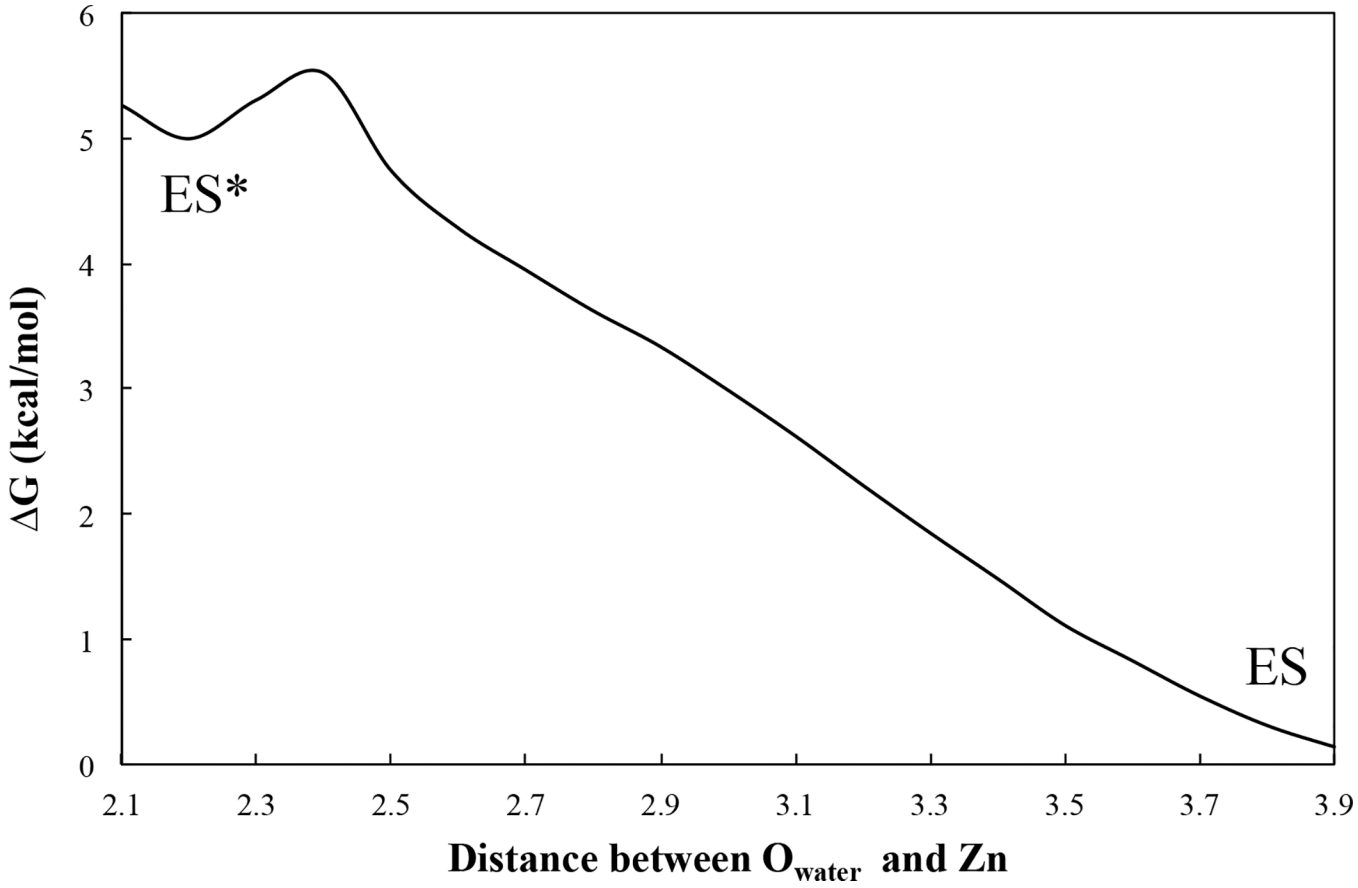

Figure 5.

QM/MM DFTB3 thermodynamic integration free energy simulation from state ES to ES* with the reduction of distance between O atom of water molecule and Zn^{2+} ion from 3.9 Å to 2.1 Å.

Table 1.

Key Zn-ligand distances (Å) in the QM/MM MP2 optimized structures A, B and C shown in Figure 2. The relative energies (ΔE) are from QM/MM MP2/[aug-cc-pVDZ/6–31G*] geometry optimization. The distances in the X-ray structure 4M1C are also included for comparison.

	ΔE (kcal/mol)	Zn-N_{His108}	Zn-N_{His112}	Zn-$O_{1,\ Glu189}$	Zn-$O_{2,\ Glu189}$	Zn-O_{Phe19}
4M1C.PDB	NA	2.331	2.121	2.258	2.682	2.199
Structure A	0.00	1.967	1.994	1.951	2.473	2.027
Structure B	8.79	1.973	1.986	1.973	2.377	2.049
Structure C	7.41	2.016	2.013	1.973	2.466	3.372